On the Double-Arcing Phenomenon in a Cutting Arc Torch

Leandro Prevosto[1], Héctor Kelly[1,2] and Beatriz Mancinelli[1]
[1]Grupo de Descargas Eléctricas, Departamento Ing. Electromecánica, Facultad Regional Venado Tuerto (UTN), Laprida 651, Venado Tuerto (2600), Santa Fe
[2]Instituto de Física del Plasma (CONICET), Departamento de Física, Facultad de Ciencias Exactas y Naturales (UBA) Ciudad Universitaria Pab. I, (1428), Buenos Aires
Argentina

1. Introduction

Transferred arc plasma torches are widely used in industrial cutting process of metallic materials because of their ability to cut almost any metal and the very high productivity that can be achieved with this technology (Boulos et al., 1994).

The plasma cutting process is characterized by a transferred electric arc that is established between a cathode, which is a part of the cutting torch, and a work-piece (the metal to be cut) acting as the anode. In order to obtain a high-quality cut, the plasma jet must be as collimated as possible and also must have a high power density. To this end, the transferred arc is constricted by a metallic tube (a nozzle) with a small inner diameter (of the order of one millimeter). Usually, a vortex-type flow with large axial and azimuthal velocity components is forced through the nozzle to provide arc stability and to protect its inner wall. In such case the hot arc is confined to the center of the nozzle, while centrifugal forces drive the colder fluid towards the nozzle walls, which are thus thermally protected. The axial component of the gas flow continuously supplies cold fluid, providing an intense convective cooling at the arc fringes. In addition, the vortex flow enhances the power dissipation per unit length of the arc column, resulting in high temperatures at the arc axis. Since the nozzle is subjected to a very high heat flux, it is made of a metal with a high thermal conductivity (copper is broadly used). The arc current is of the order of ten up to a few hundred amperes, and the gas pressure is several atmospheres. Arc axis temperatures around 15 kK are usual, but larger values, close to 25 kK or even higher, have been reached. A typical configuration of a cutting torch is presented in Fig. 1(a).

The most explored region of plasma in an arc cutting system is the arc column located between the nozzle exit and the work-piece. The experimental data from that region are obtained usually by non-invasive spectroscopic techniques (Girard et at., 2006; Peters et al., 2007; Freton et al., 2002, 2003; Pardo et al., 1999). Recently, also Langmuir probes have been used for plasma diagnostics in this kind of arcs (Prevosto et al., 2008a, 2008b, 2009a). However, due to the smallness of the nozzle bore, and the hostile conditions occurring inside such arcs, access to experimental information about the plasma state inside the nozzle region is out of reach to most plasma diagnostics; thus the published experimental data on the arc column located between the cathode and the nozzle exit are very scarce (Prevosto et

al., 2009b). Numerical simulations are usually used to study this region. However, most of the developed numerical simulations are based on the plasma local thermodynamic equilibrium (LTE) assumption (Freton et al., 2002, 2003; Gonzalez-Aguilar et al., 1999), in spite of the fact that substantial deviations from LTE should occur at the arc boundary inside the torch, where the electron density is presumably much lower than that prescribed by the Griem´s criterion for LTE equilibrium (Boulos et al., 1994); and where very high temperature gradients may be present over the last few electron Debye lengths from the nozzle wall. Only recently, a non- local thermodynamic equilibrium (NLTE) modelling of a 200 A oxygen-plasma cutting torch was presented (Ghorui et al., 2007). In this work, it was shown that the electron temperature remained high near the nozzle wall and hence well decoupled from the heavy particle temperature. For instance, an electron temperature of about 12000 K was reported for the arc boundary at the nozzle exit (a value much higher than the heavy particle temperature of about 1000 K close to the inner nozzle wall temperature).

The problem of sheath formation at the plasma boundary is of importance for nearly all applications where the plasma is confined totally or partially to a finite volume by solid walls – as in the case of cutting torch nozzles–(Riemann, 1991). When a plasma is in contact with a negatively biased surface (with a biasing voltage of the order or lower than the floating value), a strong electric field appears between the NLTE plasma and that surface. This sheath becomes positively charged, rejecting electrons from the plasma and attracting ions to the negatively biased wall. The typical thickness of the sheath as compared with the characteristic lengths of the plasma (e.g., ion mean-free-path) determines the collisional degree of the sheath. Three regimes of sheath behavior can appear in high pressure plasmas. There is a collision-dominated (i.e., mobility limited) regime when the sheath thickness is larger than the ion mean free path, a collisionless regime when the sheath is very thin, and a transition regime when both lengths are comparable. For the collision-dominated regime, expressions that describe the sheath have been developed for both the cases of constant ion mean-free-path, and constant ion mobility (Franklin, 2002a; Riemann, 2003; Sheridan & Goeckner, 1995). In the opposite limit, when ion collisions are negligible, Child's law gives a simple description of the sheath (Raizer, 1991). The number of ion mean-free-paths in the sheath needed to cause the transition from the collisionless to the collision-dominated regime for the constant mean-free-path model is only about one-half (Sheridan & Goree, 1991).

For high-pressure weakly ionized plasmas the sheath thickness is usually large compared with the ion mean-free-path, and the sheath is collision-dominated. Such a picture corresponds to the space-charge sheath formed between the NLTE plasma and the nozzle wall inside of a cutting torch because, as it will be shown later, the electron temperature is low. Near the plasma-sheath boundary the electric field accelerating the ions toward the walls is negligible. Thus the fluid velocity of the ions is small as compared to their thermal motion and the collision frequency is independent of the ion fluid velocity. On the other hand, well inside the sheath region, the electric field accelerates the ions to velocities comparable or larger than its thermal speed, and the collision frequency becomes proportional to the ion drift velocity. There is a smooth transition from a constant collision frequency of the ions within the plasma at the sheath edge to an approximately constant mean-free-path of the ions at the sheath region close to the wall where a high electric field exists. A smooth transition between these two ion collision approximations appears where the potential drop over an ion mean-free-path becomes comparable to the ion thermal energy (Sternovsky & Robertson, 2006).

In the normal mode of operation –Fig. 1(a)–, the nozzle is a floating conductor (i.e., it is not electrically connected to any part of the torch electric circuit). However, such operating mode is somewhat unstable. The much higher electrical conductivity of the nozzle as compared with that of the confined arc column would cause instability. Under certain operating conditions (too large arc current, too small gas mass flow, or a nozzle with a too small bore diameter or with a too large length) the level of arc stabilization provided by the vortex flow can be insufficient and the arc, which normally connects the cathode and the work-piece, is broken into two. One of them connects the cathode with the nozzle and the other connects the nozzle with the anode –see Fig. 1(b)–; following the path of smallest electrical resistance. Such type of arc instability is called double-arcing. From a practical point of view, the double-arcing is very undesirable; since the arc roots on the nozzle wall (especially that corresponding to the arc originated from the cathode) usually destroy the nozzle almost instantaneously (Nemchinsky & Severance, 2006). However, in a recent review (Colombo et al, 2009); high-speed images of a "non-destructive" double-arcing with a short duration (< 1 ms) were registered in cutting torches at low gas flow rates.
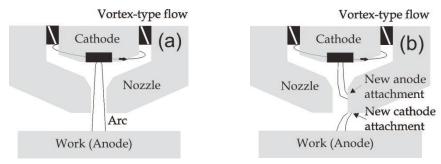

Fig. 1. Normal (a) and double-arcing (b) modes of nozzle operation of transferred arc cutting torch.

The aim of this chapter is to presents a comprehensive study of the double-arcing phenomenon which, as quoted above, is one of the main drawbacks that put limits to increasing capabilities of the plasma arc cutting process. Surprisingly, relatively little has been done to explore and understand this process, keeping in mind that the double-arcing is common not only to arc cutting but to other industrial processes as well. Section 2 presents some hypothesis suggested in the literature on the physical mechanism that triggers the double-arcing in cutting torches. In Section 3, an experimental study carried out by the authors is presented. The starting point for such a study is the analysis and interpretation of the nozzle current-voltage characteristic curve. Since there is no comprehensive theory for interpreting the electron branch in highly collisional plasmas, only the ion branch is analyzed. The influence of the collisions on the physical structure of the plasma-nozzle transition has been considered under the typical assumption of constant ion mean free path. Within this assumption and using an approximate analytical solution for the sheath thickness, the value of the ion flux to the wall is related to the nozzle voltage and the electron temperature and density at the plasma boundary. To describe the plasma composition an appropriate non-equilibrium two-temperature statistical model was used. A physical interpretation on the origin of the double-arcing phenomenon is presented, that explains why the double-arcing (that it is established when the space-charge sheath adjacent

to the nozzle wall breaks-down) appears for example at low values of the gas mass flow. A complementary numerical study of the space-charge sheath formed between the plasma and the nozzle wall of a cutting torch is also reported in Section 4. The numerical study corresponds to a collision-dominated model (ion mobility-limited motion) for the hydrodynamic description of the sheath adjacent to the nozzle wall inside of a cutting torch. The model does not assume cold ions so drift-diffusion type equations are used. Also an improved expression for the ion-neutral momentum transfer is employed, instead of the classical ion collision approximations (constant ion mean free path, and constant ion collision frequency). The ion and electron densities, electrostatic potential and ion velocity distributions are calculated inside the sheath. Boundary conditions for the numerical solutions within this sheath are based on experimental plasma data previously obtained by the authors. A physical explanation on the origin of the transient double-arcing (the so called non-destructive double-arcing) in cutting torches is reported in Section 5. Against to the proposed hypothesis (Colombo et al., 2009; Nemchinsky 2009) which assumes a transient arc voltage rise due to dielectric films deposited on the nozzle surface (which are later either carried away by the gas flow or are burned out); the experimental observations suggest that such a phenomenon is related with a strong dynamics of the space-charge sheath contiguous to the nozzle due to the arc power source ripple. Conclusions are summarized in Section 6.

2. On the physical mechanism that triggers the double-arcing in a cutting torch

In practice, a double-arcing event is seen to occur when some of the following conditions are accomplished:
(1) the arc current is too high, and/or
(2) the nozzle bore is too narrow, and/or
(3) the nozzle is too large, and/or
(4) the gas flow is too low and/or
(5) the gas flow does not have enough swirl.
Under conditions (1)-(5), the arc voltage drop inside the nozzle is high, especially when the arc current is highly constricted or the nozzle is large. For example, in a 30 A high-energy density cutting torch as is shown in Fig. 2, the measured electric field value (an average along the nozzle) is about of 11 V/mm, resulting in an arc voltage drop about of 50 V.
Before double-arcing conditions, the total current to the nozzle is zero, since the nozzle is electrically floating. However, as the whole nozzle is at a constant voltage (equipotential), each axial portion of the nozzle surface is facing an arc portion with different plasma voltage. This means that the voltage drop between the arc and the nozzle surface varies in the axial direction, and hence some portions of the nozzle surface can be collecting ions while other axial portions will collect electrons. This situation does not alter the floating character of the nozzle, because the zero current balance is fulfilled not locally (by an ambipolar flux to the nozzle), but globally on the whole body of the nozzle. Furthermore, taking into account the fact that the electrical current is almost carried by electrons, the electron collecting section of the nozzle will be very short compared to the ion collecting section. This implies that the nozzle floating potential must be close to the arc voltage at the nozzle inlet. Hence, the voltage drop between the metallic nozzle and the plasma at the nozzle exit will reach a value very close to the total arc voltage drop inside the nozzle (estimated in the previous example in about 50 V).

It has been suggested in several published works (Nemchinsky, 1998; Prevosto et al, 2009b, 2009c) that the reason for double-arcing is the high voltage drop inside the nozzle. However, the specific mechanism that triggers the double-arcing event is less clear. It was suggested (Nemchinsky, 1998; Nemchinsky & Severance, 2006) that the voltage drop inside the nozzle is concentrated across the gas envelope (i.e., the cold quasi-neutral plasma layer) that separates the hot plasma and the nozzle. In particular, in the above quoted operation conditions–(1) to (5)–, the thickness of the cold envelope could be very low and the plasma voltage drop inside the nozzle will be high. Therefore, the plasma-nozzle voltage drop will also be high (especially at axial positions close to the nozzle exit) and the electric field strength inside the cold envelope could be very close to the threshold value necessary to develop a Townsend avalanche, triggering the double-arcing. However, some experimental results (Prevosto et al., 2009b) suggest that the voltage drop inside the nozzle is concentrated in the space charge sheath formed between the quasi-neutral plasma and the nozzle wall and not in the quasi-neutral plasma, as it was previously suggested. Furthermore, a complementary numerical approach for describing the sheath structure (Prevosto et al., 2009c), suggest a possible breakdown mechanism based on the local electric field strength intensification at the nozzle wall close to the bore exit. This enhanced field could be strong enough to trigger a breakdown even if the average electric field across the sheath is not strong enough. Recently (Nemchinsky, 2009), it was proposed another breakdown mechanism where dielectric films deposited on the nozzle wall would play a key role. Such a mechanism explains the relative ease of double-arcing with worn consumables (cathode and nozzle). However, experimental evidence is required to support (or disapprove) such hypothesis.

3. An experiment to infer the plasma-nozzle sheath structure

3.1 Experimental details
The metallic nozzle that bounds the arc can be considered itself as a large-sized Langmuir probe, and hence it can be used to collect charges from the contiguous plasma (i.e., to build the current-voltage characteristic curve of the nozzle) and therefore to obtain information about the plasma state inside it. The necessary condition for a comprehensive use of the probe (that is: the plasma should not be perturbed sufficiently far away from the probe surface) is fully accomplished since the nozzle-probe behaves as a natural boundary to the arc.

To obtain the current-voltage nozzle characteristic, it was necessary to bias the nozzle (that under normal arc operation remains floating –see Fig. 1(a)–). The nozzle biasing circuit is shown in Fig. 2. Different nozzle bias voltages V_N were obtained using a high-impedance rheostat, and were registered (with respect to the grounded anode) by using a voltage meter. Alternatively, a two-channel digital oscilloscope (Tektronix TDS 1002 B) with a sampling rate of 500 MS/s and a analogical bandwidth of 60 MHz was used to register eventual fluctuations induced by the arc power source ripple. The nozzle current i was calculated from the voltage drop V_0 through a small resistance R_0. Alternatively, the nozzle was disconnected to perform nozzle floating voltage measurements. To determine the plasma floating potential close to the nozzle exit, sweeping electrostatic probes previously developed (Prevosto et al., 2008a) were employed.

Experiments were conducted using a high-energy density cutting torch as is shown in Fig. 2. It consists of a cathode centered above an orifice in a converging-straight copper nozzle

without liquid cooling. The cathode was made of copper (7 mm in diameter) with a hafnium tip (1.5 mm in diameter) inserted at the cathode center. A flow of oxygen gas cooled the cathode and the nozzle and was also employed as the plasma gas. The gas passed through a swirl ring to provide arc stability. The nozzle consisted in a converging-straight bore (with a bore radius R_N = 0.5 mm and a length L_N = 4.5 mm) in a copper holder surrounding the cathode (with a separation of 0.5 mm between the holder and the cathode surface). To avoid plasma contamination by metal vapors from the anode, a rotating steel disk with 200 mm in diameter and 15 mm thickness was used as the anode (Ramakrishnan et al., 1997). In this study, the disk upper surface was located at 5 mm from the nozzle exit. The arc was transferred to the edge of the disk, and the rotating frequency of the disk was equal to 29.5 Hz. At this velocity, a well-stabilized arc column was obtained, and the lateral surface of the anode disc was completely not melted. Thus, practically no metal vapors from the anode were present in the arc. A 3-phase transductor type of power supply with a root-mean-square (RMS) ripple value of 7 % was used to run the torch. The ripple level was eventually reduced to 3 % (RMS value) by using a high-impedance inductor choke. The fundamental ripple frequency was in all the cases 150 Hz. The measured arc torch operating conditions were: the arc current I, the chamber pressure (p_{ch}) and the gas mass flow rate ($\dot{m}$). During the experiments the arc current was fixed at 30 A.
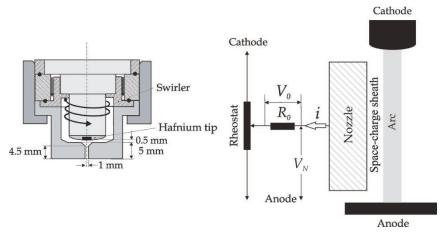

Fig. 2. Scheme of the biasing nozzle circuit and the physical structure of the plasma contiguous to the nozzle surface (right). At the left a schematic of the arc torch indicating several geometric dimensions is also presented.

3.2 Experimental data

A typical current–voltage nozzle characteristic curve (with the electron current considered as positive) based on the voltage meter measurements (i.e., –RMS– values of i and V_N) is shown in Fig. 3. This figure corresponds to $\dot{m} = 0.54 \, \mathrm{g\,s}^{-1}$, p_{ch} = 0.65 MPa and a power source ripple level of 3 %. A detail of the ion branch with an enlarged current scale is shown. For comparison purposes the ion branches corresponding to other $\dot{m}$ values have been included in Fig. 3. The intersection points of the ion branches with the zero-current line (i.e., the nozzle floating voltage values) are clearly identified. For the smallest $\dot{m}$ value double-

arcing was found for V_N = -155 ± 5 V. Using a well-known relationship between the floating and plasma potential (Raizer, 1997), that establishes that the difference between these two potentials is a linear function of the electron temperature, it is possible to derive the plasma potential. For the electron temperature range of interest (12000 to 16000) K (Prevosto et al., 2008b), and from the plasma floating value at the nozzle exit obtained with the electrostatic probe under this operating condition (= -30 ± 3 V); a plasma potential value of ≈ -22 V was obtained.

Fig. 3. Nozzle i-V_N characteristic for the largest gas mass flow used. A detail of the ion branches for several gas mass flow values is also shown. Taken from Prevosto et al., 2009b.

From Fig. 3, note also that the largest electron current drained from the arc is relatively small ≈ 1 A, notwithstanding the fact that the size of the nozzle is quite large. This fact reflects the existence of a very low electron density close to the nozzle wall. Also note the great difference between the intensities of the ion and electron collected currents, indicating that in this experimental conditions electron attachment is not significant. These features were common to all the $\dot{m}$ values investigated. Concerning to the ion branches shown in Fig. 3, note that the current drained by the nozzle increases when $\dot{m}$ decreases. Also note that no ion saturation current was found. This behaviour is similar to those presented in wall-stabilized arc experiments with (Hill & Jones, 1979) or without externally imposed axial gas flow (George & Richards, 1968)

3.3 Data interpretation

As quoted before, it has been suggested that the double-arcing is triggered by the high voltage drop inside the nozzle. From Fig. 3 a total voltage drop of 133 ± 5 V can be derived as the voltage breakdown value at the nozzle exit for $\dot{m} = 0.32\,\mathrm{g\,s^{-1}}$. That voltage drop results from a plasma potential of - 22 V minus a nozzle voltage of – 155 V. For the other larger investigated $\dot{m}$ values the nozzle voltage could be lowered up to values very close to

the cathode voltage without evidence of any breakdown. According to Paschen's law (Raizer, 1997) the breakdown voltage value depends on the gas layer thickness D times the gas density n_n. A reasonable estimation of n_n at the nozzle exit can be obtained by taking an outer value of 0.1 MPa for the gas pressure and by assuming a heavy particle (gas) temperature T_h close to the estimated nozzle inner wall temperature ($T_h \approx 1000$ K). Therefore, neglecting the plasma pressure (this assumption will be verified later in this chapter) it results $n_n \approx 7.2 \times 10^{24}$ m^{-3}. Using the inferred n_n value and the total voltage drop (133 V) across the gas layer thickness together with the experimentally determined Paschen's law for an oxygen gas (Hackam, 1969), a threshold value $D = 20 \pm 2$ μm was determined at the nozzle exit. This means that for sheath thickness equal or shorter than that threshold breakdown will occur between the arc plasma edge and the nozzle, thus triggering the double-arcing. To relate D with the plasma characteristic it was assumed that D corresponds to the thickness of the electrical boundary layer that appears between the unperturbed plasma and the nozzle wall. Such an assumption will be later verified.

Due to the high operating gas pressure values and the relatively low electron density (n_e) at the plasma boundary, we will also assume that this layer is fully-collisional. When the sheath is collisional and without ionization (because both, the electron density and the thickness of the sheath are small), there is a smooth joining between the plasma and the space-charge layer without the need of introducing a transitional sheath (i.e., the pre-sheath) (Blank, 1968; Franklin, 2003a, 2003b, 2004). The thickness of such a fully-collisional space-charge layer that appears between the nozzle wall and the NLTE plasma in a cutting torch can be approximated in terms of the plasma-wall voltage drop ($\Delta V \circ V_N$ - V_p where V_p is the plasma potential.) as (Sheridan & Goree, 1991)

$$D \gg 2.2 \times 10^4 \, \Delta V^{3/5} \, n_e^{-1/2} \, T_e^{-1/10} \,, \tag{1}$$

where all the physical variables are given in MKS units (T_e is the electron temperature). In NLTE plasmas, when the particle population in the different energy levels is still dominated by electron collisions, the non-equilibrium generalized Saha-equation (van de Sanden et al., 1989) is appropriate to describe the composition of the quasi-neutral plasma. For the first ionization

$$\frac{n_e n_i}{n_n} = 2 \frac{Q_i}{Q_0} \left(\frac{2\pi m k T_e}{h^2} \right)^{3/2} \exp\left(-\frac{E_I}{k T_e} \right), \tag{2}$$

(where n_i is the ion density, Q_i and Q_o are the statistical weights of oxygen ions and atoms, m is the electron mass, k is the Boltzmann's constant, h is the Planck's constant and E_I is the ionization energy of the oxygen atoms). Also the neutrality equation can be used for the unperturbed plasma region at the sheath edge,

$$n_e \approx n_i \,. \tag{3}$$

Employing the derived threshold D value, together with the already calculated neutral gas density ($n_n \approx 7.2 \times 10^{24}$ m^{-3}) and the equations (1) to (3); the plasma values T_e and n_e (evaluated at the sheath edge) at the nozzle exit are $n_e \approx 7.5 \times 10^{19}$ m^{-3} and $T_e \approx 5700$ K. Note

that the obtained value for n_e is well below the lower limiting value to apply local thermodynamic equilibrium in accord with Griem's criterion ($\geq 10^{23}\,\mathrm{m}^{-3}$). Also note that in this region the plasma pressure ($kn_e(T_e + T_h) \approx 10\,\mathrm{Pa}$) results much lower than the gas pressure, which justify the assumption made in the estimation of the gas density at the nozzle exit.

The physical picture presented up to now can be used to look for an explanation of the behaviour of the nozzle ion branch characteristic. The ion current (i_+) collected by the nozzle can be written as

$$i_+ = 2\pi R_N\, e \int_{z=0}^{z=L_N} n_{is}\, u_{is}\, dz \qquad (4)$$

where z is the coordinate directed along the nozzle wall and the ion density and velocity must be evaluated at the sheath edge. Due to the collisional regime of the sheath, the ion entrance velocity is (Franklin, 2002b)

$$u_{is} \approx u_B \left(\lambda_+ / \lambda_{Ds} \right)^{1/2}, \qquad (5)$$

which is lower than the Bohm velocity (u_B). (λ_+ is the collisional ion mean free path and λ_{Ds} is the electron Debye length at the layer entrance). It should be noted that because the sheath thickness depends on the nozzle voltage value –equation (1)–, the presented physical picture suggest that a larger ΔV value produces a thicker sheath and hence the plasma is "probed" at different radial positions producing different current values to the nozzle. This fact explains the lack of saturation in the ion branch. It is interesting to note that, since the expected values of T_e are around 5000-6000 K (according to what was found with the breakdown estimation), the generalized Saha equation (2) predicts a very strong dependence of n_e on T_e, thus resulting in very small variations of T_e that are able to produce large enough variations of n_e that in turn can explain the behaviour of the characteristic. In order to invert equation (4), the z-dependence of the integrand must be known. To do this, the following assumptions were made: 1) a linear variation of the pressure (p) and V_p on z, 2) a constant value for T_e in the axial direction (an average along the nozzle length) at a radial position close to the nozzle wall.

Assumptions 1) and 2) have been shown to be valid in cutting torches (Pardo et al., 1999; Freton et al., 2002; Ghorui et al., 2007). In any case, the obtained solution is almost insensitive to the particular chosen variations of p since the dependence of the integral in equation (4) with n_n is very weak (leading to a dependence of the kind $n_n^{1/8}$). To calculate the electrostatic potential of the plasma it is necessary to know its value in two different axial positions. Both values have been previously inferred from the experiments. For instance for $\dot{m} = 0.32\,\mathrm{g\,s}^{-1}$ the values of V_p are: $V_p(z=L) \approx -22\,\mathrm{V}$ and $V_p(z=0) \approx -70\,\mathrm{V}$ (see Fig. 3). The resulting value of the constant axial electric field in this case is 11 V/mm. From assumption 2) T_e only depends on the radial coordinate r and it can written in a simple form as a polynomial expansion

$$T_e(r) = a_0 + a_1\, r + a_2\, r^2 + ... + a_{q-1}\, r^{q-1}, \qquad (6)$$

where $a_0, a_1, ..., a_{q-1}$ are q unknown constant numerical coefficients. Then replacing n_e in terms of T_e (evaluated at the sheath edge $T_e(r = R_N - D)$) through Saha equation in equation (1), the z dependence of the sheath thickness D as a function of the quoted unknown q numerical coefficients is found. Hence equation (4) can be integrated for q points of the ion branch characteristic to produce a closed system of equations.

It should be noted that in this kind of cutting torches, the arc is extremely constricted, resulting in high pressures, high current densities and correspondingly high temperatures on the arc axis. So the radiative arc loses are a significant fraction of the electrical power input with a strong contribution in the UV range (Shayler & Fang, 1978). Using the NEC model (Naghizadeh-Kashani et al., 2002) for an atmospheric pressure oxygen plasma, and a copper photoemission coefficient $\gamma_v \approx 10^{-4}$ (Dowell et al., 2006); the maximum photoelectron current from the nozzle surface results $\approx$ 10 mA. This photoelectron current will not depend on the nozzle voltage, and only could produce a change in the characteristic curves at the vicinities of the nozzle floating voltage value (see Fig. 3). For this reason, the characteristic region near the floating voltage was not considered in the inversion of equation (4). With all these considerations, and using the well-known Chebyshev formula (Noble, 1964) to approximate the integrals of this system of equations, the inversion problem finally can be solved calculating the solution of the $q \times q$ system of equations in terms of the q numerical coefficients in equation (6). Thus the $T_e(r)$ profile that fits the characteristic ion branch in the radial range cover for the D values was found.

In practice for all the studied cases, a linear variation of $T_e(r)$ was found sufficient to fit the characteristic ion branches within the experimental uncertainty ($\approx$ 5%), resulting mainly from statistical fluctuations of the current and voltage RMS values.

In Fig. 4 $D(z)$ for the different $\dot{m}$ values and for the largest nozzle voltage value registered in each characteristic ion branch is presented. It can be seen that for the lowest gas mass flow value ($\dot{m} = 0.32\,\text{g s}^{-1}$) an almost constant $D(z) \approx 21\,\mu\text{m}$ results. Note that the gas layer thickness at the nozzle exit value ($\approx$ 20 ± 2 μm) inferred from the voltage breakdown measurement for this case is quite close to the predicted space-charge sheath thickness value (thus supporting the hypothesis of that the voltage drop inside the nozzle is concentrated in the space-charge layer, and not in the quasi-neutral plasma). In the other cases, a more marked increase with z appears in $D(z)$, varying in the range 26 to 30 μm for $\dot{m} = 0.43\,\text{g s}^{-1}$ and 27 to 31 μm for $\dot{m} = 0.54\,\text{g s}^{-1}$. These values are higher than the sheath thickness value corresponding to the lowest gas mass flow case, which is consistent with the absence of breakdown found in these cases. Concerning the validity of the colisional sheath assumption, the ratio of the sheath thickness to the ion mean free path results $D/\lambda_+ \approx 100$, showing that the above-mentioned assumption is fully satisfied.

In Fig. 5 the radial profiles of T_e corresponding to the registered ion branch characteristics are presented as a function of the radial coordinate measured from the nozzle wall ($R_N - r$). Fig. 5 shows that the values of T_e for the different $\dot{m}$ values are not very different (4700 to 5700 K), but there appear large and quite different T_e radial gradients. In fact, gradients of the order of 0.9 to 1.1 × 10⁸ K m⁻¹ for 0.43 to 0.54 g s⁻¹ and 1.1 × 10⁹ K m⁻¹ for 0.32 gs⁻¹ are found very close to the nozzle wall, thus supporting the assumption of the lack of LTE.
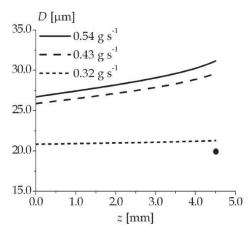
Fig. 4. Sheath thickness along the nozzle wall for the largest nozzle voltage value experimentally registered for each gas mass flow value. For comparative purposes, the black circle indicates the sheath thickness value inferred at the nozzle exit using the voltage breakdown measurement. Taken from Prevosto et al., 2009b.
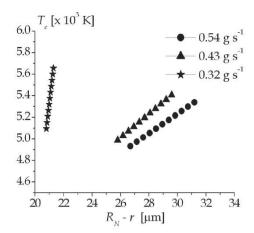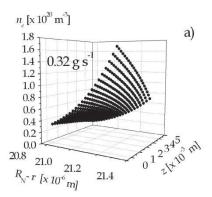

Fig. 5. Radial profiles of the average (along the nozzle wall) plasma electron temperature as a function of the radial position measured from the nozzle wall, for the different gas mass flow values. Taken from Prevosto et al., 2009b.

The spatial distribution of the plasma density is presented in Figs. 6a) and b), for a gas mass flow rate of 0.32 g s^{-1} and 0.54 g s^{-1}, respectively. A steep plasma density radial gradient is shown in Fig. 6a) due to the existence of very large electron temperature radial gradient close to the nozzle wall (see Fig. 5). Less marked plasma density gradients close to the nozzle wall are shown in Fig. 6b) for the largest gas mass flow rate registered. In both figures, the existence of a plasma pressure gradient along the nozzle produces the axial variation in the plasma density.
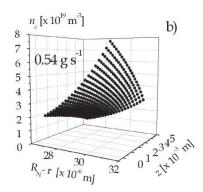
Fig. 6. a) Spatial distribution of the plasma density close to the nozzle wall for the lowest gas mass flow experimentally registered. b) Spatial distribution of the plasma density close to the nozzle wall for the largest gas mass flow experimentally registered. Taken from Prevosto et al., 2009b.

According to the experimental and theoretical results given above by Figs. 3 to 6, the physical structure of the electrical boundary layer is strongly influenced by the gas mass flow rate. The experimental results varying the $\dot{m}$ value show that the current drained by the nozzle increases (see Fig. 3) when the gas mass flow decreases until finally a breakdown appears, (see Figs. 4 to 6), in the sense that the T_e profile critically depends on the $\dot{m}$ value. When the $\dot{m}$ value decreases, very large T_e radial gradients (of the order of 10^9 K m^{-1}) produce (through Saha equation) steep n_e radial gradients over the last few Debye electron lengths from the nozzle wall. As a result, the sheath thickness is almost independent on the ΔV value, producing an almost constant (and thin) sheath thickness along the nozzle for low $\dot{m}$ values. Once the sheath thickness is smaller than the critical value, the space-charge sheath breaks-down leading to double-arcing. A good agreement between the critical value of the D thickness at the nozzle exit inferred from the voltage breakdown (under the Townsend breakdown hypothesis) and the predicted value was found.

4. Numerical model to describe the plasma-nozzle sheath structure at large negative bias voltages

4.1 Collisional sheath model

As quoted in Section 3, when both plasma and sheath are collisional, and when the ionization inside the sheath can be neglected, there is a smooth joining between the plasma and the space-charge layer, thus avoiding the need of the presence of a transitional sheath (the so called pre-sheath). Thus, the sheath edge coincides with the unperturbed quasi-neutral plasma. The model geometry showing the collisional space-charge sheath contiguous to the negatively biased nozzle is sketched in Fig. 7. Since the sheath remains thin as compared with the nozzle bore size (see Fig. 4) a planar geometry is used (y and x are the normal and axial coordinates with respect to the nozzle wall, see Fig. 7). At negative nozzle potentials (of the order or lower than the floating value), the electron density within the positive sheath remains small as compared to the ion density, so ionizations inside the sheath can be ignored. The elastic mean-free-paths for all species are much smaller than the sheath thickness, and therefore the fluid description applies. Steady-state conditions are assumed.

The governing equations (Goldston & Rutherford, 1995) are given by the ion continuity equation

$$\nabla \cdot \left(n_i \, \overline{u}_i \right) = 0 \, , \tag{7}$$

the electron continuity equation

$$\nabla \cdot \left(n_e \, \overline{u}_e \right) = 0 \, , \tag{8}$$

the ion momentum equation

$$n_i \, M \left(\overline{u}_i \cdot \nabla \right) \overline{u}_i = - \nabla \left(n_i \, k T_h \right) - e \, n_i \, \nabla V_p + n_i \, M \left(\overline{u}_n - \overline{u}_i \right) \nu_i \, , \tag{9}$$

where $\overline{u}_e$ is the electron fluid velocity, M is the ion mass and e the electron charge. The last term of equation (9) represents the drag force due to the collisions between ions and neutrals. $\overline{u}_n$ is the neutral fluid velocity and ν_i the ion-neutral collision frequency for momentum transfer.

The electron momentum equation

$$n_e \, m \left(\overline{u}_e \cdot \nabla \right) \overline{u}_e = - \nabla \left(n_e \, k T_e \right) + e \, n_e \, \nabla V_p - n_e \, m \, \overline{u}_e \, \nu_m \, , \tag{10}$$

where ν_m is the effective collision frequency for momentum transfer. Finally, Poisson's equation relates the difference between ion and electron densities within the sheath to the self-consistent potential

$$\varepsilon_0 \, \nabla^2 V_p = - e \left(n_i - n_e \right) , \tag{11}$$

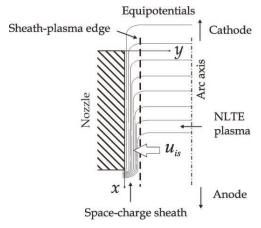where ε_0 is the vacuum permittivity.

Fig. 7. Schematic of the sheath formed between the NLTE plasma and the nozzle wall. Taken from Prevosto et al., 2009c.

The inertial term can be safely dropped from equation (10) because of the smallness of the electron mass. Considering the Einstein relation equation (10) reduces to the total electron flux (Raizer, 1991)

$$\overline{\Gamma}_e \equiv n_e \overline{u}_e = n_e \mu_e \nabla V_p - D_e \nabla n_e , \tag{12}$$

where the usually small thermo-diffusion term (proportional to $-\nabla T_e$) was neglected in equation (10) as compared to the diffusion term (Raizer, 1991). μ_e and D_e are the electron mobility and diffusion coefficients. If the nozzle potential is sufficiently negative, due to the high mobility of the electrons, oppositely directed high diffusion and drift electron fluxes approximately balance each other to yield a small resultant total electron flux, comparable with (or less than) the ion flux. Hence $\overline{\Gamma}_e \approx 0$ in equation (12) and the electron density inside the sheath obeys the relation

$$n_e = n_{es} \exp\left[\frac{e(V_p - V_{ps})}{kT_e} \right], \tag{13}$$

where n_{es} and V_{ps} are the density and the electrostatic potential of the plasma at the sheath-plasma edge. The neutral particles are considered at rest (i.e. $u_i \gg u_n$). To close the model, an expression for the ion momentum transfer by elastic collisions must be established. Two special cases are usually treated in the literature (Franklin, 2002a; Riemann, 2003): constant ion mean-free-path and constant ion collision frequency. In the first case, the basic assumption is $e|\nabla V_p|\lambda_i \gg kT_h$, which means that the ion drift velocity is much larger than the ion thermal velocity. Hence the drag force is modeled by $-Mu_i\overline{u}/\lambda_i$, where the ion mean-free-path $\lambda_i \equiv (n_n \sigma)^{-1}$ is constant (σ is the momentum transfer cross section for elastic collisions between ions and neutrals). The collision frequency $\nu_i = u_i/\lambda_i$ depends in this case on the ion fluid velocity. In the opposite limit the assumption $e|\nabla V_p|\lambda_i \ll kT_h$ applies. If this condition is satisfied, the ion fluid velocity is much smaller than its thermal speed. The collision frequency of the ions is thus determined by their random thermal motion rather than their fluid velocity and thus $\nu_i = \sqrt{2}\,u_{th}/\lambda_i$. In this relation the ion thermal velocity is given as $u_{th} = \sqrt{8kT_h/(\pi M)}$, and the constant ion collision frequency is independent of the fluid velocity. The factor $2^{1/2}$ is due to the mutual motion of the ions and neutral assuming the same temperature for both species (Boulos et al., 1994). The drag force in this case is given as $-M\nu_i\overline{u}_i$. Both physical approximations assume that the collision cross section is independent of the ion fluid velocity. At high pressures, for strongly collisional sheaths, the constant ion mean-free-path approximation applies close to the wall where the electric field strength is stronger. On the other hand, the constant ion mobility approximation (constant ion collision frequency) is physically more accurate at the sheath-plasma edge (where the electric field is relatively weak). In the transition region, the collision frequency is given by $\nu_i(u_i) = \sqrt{(\nu_\lambda)^2 + (\nu_\nu)^2}$ (Sternovsky & Robertson, 2006) where ν_λ and ν_ν are the ion collision frequencies in the previously quoted approximations. Following this approach, the ion collision frequency can be written as

$$\nu_i(u_i) = \frac{\sqrt{u_i^2 + 2u_{th}^2}}{\lambda_i} . \tag{14}$$

In spite of the collisional nature of the sheath, inelastic electron collisions are very rare and also the electron energy transfer to heavy particles by elastic collisions is small. Therefore, it can be assumed that $T_e \approx$ constant inside the sheath, with a value corresponding to the sheath-plasma edge value.

The model is now closed. In the limit of strong ion-neutral collisions (i.e., the mobility-limited ion motion approximation) the collision parameter D/λ_i is large as was shown in Subsection 3.3. In such circumstances equation (9) is simplified by neglecting the convective term on its left hand side. Combining equations (7), (9), (11), (13) and (14), a system of coupled partial differential equations for describing the mobility-limited ion colisional sheath was obtained.

$$\frac{\partial\left(n_i u_{ix}\right)}{\partial x} + \frac{\partial\left(n_i u_{iy}\right)}{\partial y} = 0 \, , \tag{15}$$

$$-\frac{\partial\left(n_i k T_h\right)}{\partial x} - e n_i \frac{\partial V_p}{\partial x} - n_i M u_{ix} \nu_i = 0 \, , \tag{16}$$

$$-\frac{\partial\left(n_i k T_h\right)}{\partial y} - e n_i \frac{\partial V_p}{\partial y} - n_i M u_{iy} \nu_i = 0 \, , \tag{17}$$

$$\frac{\partial^2 V_p}{\partial x^2} + \frac{\partial^2 V_p}{\partial y^2} = -\frac{e}{\varepsilon_0} n_{is}\left[\frac{n_i}{n_{is}} - \exp\left(\frac{e\left(V_p - V_{ps}\right)}{k T_e}\right)\right] \, , \tag{18}$$

where the ion collision frequency is given by equation (14). A similar plasma sheath model was presented (Sheridan & Goree, 1991) for a two-fluid ($T_h \ll T_e$, i.e. cold ions) uniform plasma but under the above quoted extreme collisional approximations. The present model is further complicated by the axial potential drop along the arc column facing the equipotential nozzle (see Fig. 7). Also for large ion temperatures (in this problem T_h is comparable to T_e) the thermal ion flux to the wall cannot be neglected; therefore the diffusive term in equation (9) must be considered.

To solve equations (15)-(18), the appropriate boundary condition (sheath thickness, plasma density and electron temperature at the sheath-plasma edge, arc voltage and gas pressure profiles inside the nozzle) were presented in Section 3. At the nozzle wall ($y = 0$), the voltage of the nozzle is known (V_N). The sheath-plasma edge ($y = D$) coincides with the quasi-neutral plasma, so $n_{is} \equiv n_i \cong n_e$ and the voltage distribution is that of the plasma arc (variable) voltage. Also the radial electric field value at the sheath-plasma edge is very small (Raizer, 1991), hence $\partial V_p/\partial y\big)_{y=D} \approx 0$. The ions enter the sheath from the plasma with a velocity normal to the boundary surface given by $u_{is} \approx u_B\left(\lambda_i/\lambda_{Ds}\right)^{1/2}$. At the nozzle inlet ($x = 0$) and exit ($x = L_n$), open boundary conditions were assumed. So the quantities $\partial u_{ix}/\partial x$, $\partial u_{iy}/\partial x$, $\partial n_i/\partial x$ and $\partial V_p/\partial x$ are conserved through these surfaces.

4.2 Numerical results and discussion

The governing equations (8)-(12) were solved for the electric potential, ion velocity (both components) and for the ion density, by integrating them numerically using a finite difference discretization technique in a 100×50 uniform grid. An iterative method was adopted, that continued until the relative difference between two consecutive iterations of all the physical quantities was less than 10^{-5}.

To found the mechanism that triggers the undesirable sheath breakdown, the following torch operation conditions were used: arc current of 30 A, oxygen gas mass flow of 0.32 g s^{-1} and V_n = -155 V. In such conditions, a thin sheath with an almost constant thickness of $D(z)$ = 21 µm (see Fig. 4) was formed between the plasma and the nozzle wall.

Fig. 8. Spatial distribution of the electric field strength inside the sheath. Taken from Prevosto et al., 2009c.

In Fig. 8, the spatial distribution of the electric field strength is presented. As it can be seen, the electric field value is high, with the largest values along the nozzle wall, varying from 6×10^6 V m^{-1} near the nozzle entrance to about 9×10^6 V m^{-1} at the nozzle exit. This enhanced value is higher than the average field value across the sheath, and is of the order of the breakdown threshold value. This means that an undesired sheath breakdown could occur close to the nozzle exit even if the average electric field across the sheath is not strong enough.

The spatial distributions of the ion and electron densities inside the sheath are presented in Figs. 9 and 10. As it can be seen in these Figs., n_i drops sharply near the sheath edge and continues decreasing slowly, while the electron density also shows a very steep drop near the sheath edge, with a virtually zero value everywhere inside the sheath. The lack of electrons inside the sheath implies that the electron thermal conduction flux to the nozzle wall can be neglected. The nozzle wall results thus thermally isolated, in spite of the high electron temperature in its adjacency. It was found that both the ion and electron densities decrease when the electrostatic potential decreases. This behavior of n_i is due to the ion acceleration at an almost constant ion flux, while the n_e behavior is due to the fact that the electrons are related with the electric field according to a Boltzmann equation –equation 13–.
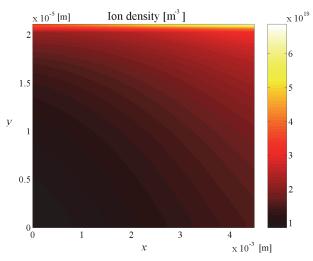
Fig. 9. Spatial distribution of n_i inside the sheath. Taken from Prevosto et al., 2009c.
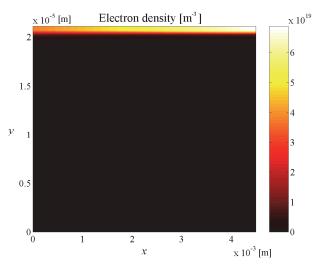

Fig. 10. Spatial distribution of n_e inside the sheath. Taken from Prevosto et al., 2009c.

5. Experimental evidence on the "non-destructive" double-arcing

In Section 1 it was mentioned that a transient (duration < 1 ms), non-destructive, double-arcing in cutting torches was recently identified (Colombo et al, 2009) by using high-speed imaging during the torch piercing phase. Gas flow rates and torch stand-off were set to increase the probability of double arcing. In Colombo's experiment, the sequence of images showed several phenomena that can be associated with the double arcing. In particular, green vapours and silver grey vapours appearing in some of the frames can be correlated

with copper (nozzle wall) and hafnium (cathode) vapour emissions, respectively. The emission of copper vapours could be the consequence of an arc attachment to the nozzle, while the hafnium vapours exiting the nozzle could be related to a greater erosion of the hafnium cathode insert in the case of double-arcing due to an arc root attachment instability on the cathode emissive surface. The high-speed double-arcing images have been time-correlated with the oscilloscope waveform of the arc voltage drop between the cathode and the nozzle, and good correspondence was found. The authors then suggested that the non-destructive double-arcing phenomena during piercing probably occur as a consequence of the deposition of a small amount of hafnium oxide on the nozzle orifice wall, which induces a local increase in the radial electric field and hence an increase in the probability of double arcing. When double arcing occurs, rapid (<1 ms) evaporation of hafnium oxide with vapour emission from the nozzle restores the previous and normal arc behaviour. Due to their very short duration, the described phenomena should have a non-destructive character.

Usually, the power sources used for run cutting torches are poorly stabilized and have large ripple factors, with RMS values that can amount to 10 % of the time-averaged arc voltages (Pardo et al, 1999; Prevosto et al., 2008a; 2008b). This is due to the fact that the arc currents in cutting torches are typically large (of the order of 100 A) which difficult an effective filtering of the ripple. If a 3-phase transductor type power supply is used, then the fundamental ripple frequency is 150 Hz and if 3-phase silicon controlled rectifier (SCR) based power supply is used, then the ripple frequency is 300 Hz. The strong oscillatory components in the voltage and arc current should produce in turn, large fluctuations in the plasma quantities that vary at the ripple frequency.
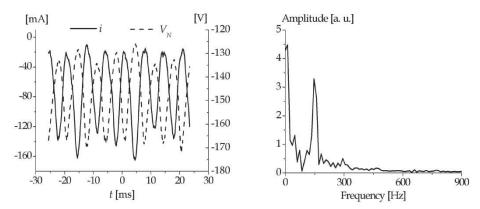

Fig. 11. Ion current and nozzle voltage waveforms for a 7 % RMS ripple level. The Fourier analysis of the ion current waveform is also shown.

Fig. 11 shows a typical V_N and i waveforms corresponding to the torch described in Section 3.1 for $\dot{m} = 0.39\,\mathrm{g\,s^{-1}}$ and a power supply ripple level of 7 %. The gas mass flow value is close to that producing double-arcing in this torch. It can be seen from Fig. 11 (left) that both waveforms exhibit high fluctuation levels, reaching for the ion current signal an amplitude (peak value) of about ≈ 75 % of the time-averaged value. Also, both waveforms are in opposite phase, a fact that could be related to a negative slope of the current–voltage

characteristic curve of this kind of arcs. The Fourier analysis of the ion current waveform (fig. 11, right) shows that the signal has a very strong component at 150 Hz, which is the fundamental frequency of the power source ripple.
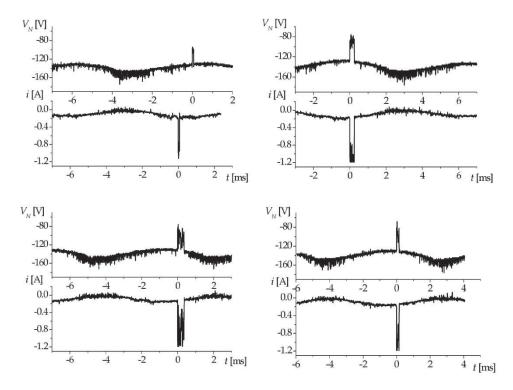

Fig. 12. Sequence of ion current and nozzle voltage waveforms with a reduced time-scale showing arc instabilities associated with the transient double-arcing phenomenon. The arc operation is close to the full-scale double-arcing.

This experimental result shows that the NLTE plasma inside the nozzle of a cutting torch results strongly affected by the arc voltage ripple, and thus it is far from the steady state, as it is usually assumed in the literature (e.g., Gonzalez-Aguilar et al., 1999; Freton et al., 2002; 2003; Ghorui et al., 2007; Zhou et al., 2009, Guo et al., 2010). Such dynamics could explain the mechanism of formation of the non-destructive double arcing; as it is shown with detail in Fig. 12. In these oscillograms (with a reduced time-scale), the ion current and nozzle voltage are shown for the same arc operating conditions (i.e., $\dot{m} = 0.39\,\mathrm{g\,s^{-1}}$ and a ripple level of 7 %). The sequence of images shows marked arc instabilities (during time intervals < 1 ms) that can be associated with the transient double-arcing phenomenon. It should be noted that such instabilities approximately coincides with the negative peak value of the ion current; thus supporting the hypothesis that the "non-destructive" double-arcing phenomenon is related to the plasma dynamics inside the nozzle. Another argument to support this hypothesis is the quite high repeatability of the phenomenon.

6. Final discussion and conclusions

In this work, we have presented a study of the arc plasma-nozzle sheath structure, which is the region where the double-arcing takes place.

The starting point was obtaining a physical interpretation of the RMS current-voltage characteristic of the nozzle that led to predict the thickness of the quoted sheath in terms of the gas mass flow value. Thus, a Towsend-type breakdown of the neutral gas inside the sheath was suggested as the double-arcing trigger. The predicted gas mass flow value that produced a breakdown was in good agreement with the experimental $\dot{m}$ that actually produced double arcing in our torch.

A detailed study of the sheath structure by developing a numerical model for a collisional sheath was also presented. This model allowed obtaining profiles of the electron and ion densities and electric field along the sheath, which confirmed the Towsend-type breakdown of the sheath as the most likely mechanism to produce double-arcing. In particular the breakdown was based on the local electric field strength intensification at the nozzle wall close to the bore exit. This enhanced field could be strong enough to trigger a breakdown even if the average electric field across de sheath is not strong enough.

The proposed mechanism is quite different from that previously found in the literature (Nemchinsky (1998) and Nemchinsky & Severance (2006)), in which it is suggested that the voltage drop inside the nozzle is concentrated across the cold quasi-neutral plasma layer that separates the hot plasma and the nozzle. Note that our hypothesis implies that the thickness of the space-charge layer (where almost all the electric field is concentrated) is shorter than the cold gas envelope (i.e., the electric field cannot penetrate deep inside such envelope), thus the average electric field in the nozzle vicinity rises ($\approx \Delta V / D$). The cold gas envelope hypothesis was recently adopted by Guo et al. (2010). Its thickness was arbitrary defined as the contour corresponding to 7000 K (≈ 0.5 mm). However, the electric field cannot penetrate inside such envelope since the space-charge layer at this temperature value is much smaller than such gas envelope.

A transient (duration < 1 ms), double-arcing in cutting torches –the so called "non-destructive" double-arcing– was recently identified (Colombo et al, 2009) under torch operating conditions close to those producing double-arcing. Similar observations of this phenomenon have been presented in this work. Due to their very short duration the described phenomena can have a non-destructive character. Although the literature proposed hypothesis (Colombo et al., 2009; Nemchinsky 2009) assumes a transient arc voltage rise due to dielectric films deposited on the nozzle surface (which are later either carried away by the gas flow or are burned out); our experimental observations suggest that such a phenomenon is more likely related with the dynamics of the space-charge sheath contiguous to the nozzle due to the arc power source ripple.
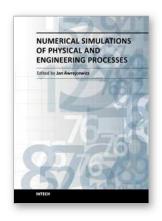
7. Acknowledgement

8. References

Blank, J. L. (1968). Collision-dominated positive column of a weakly ionized gas. *Phys. Fluids*, 11, 1686.

Boulos, M.; Fauchais, P. & Pfender, E. (1994). *Thermal Plasmas, Fundamentals and Applications*, Vol1, Plenum Press, New York.

Colombo, V.; Concetti, A.; Ghedini, E.; Dallavalle, S. & Vancini, M. (2009). High–speed imaging in plasma arc cutting: a review and new developments. *Plasma Sources Sci. Technol.*, 18, 023001.

Dowell, D. H.; King, F. K.; Kirby, R. E. & Schemerge, J. F. (2006). In situ cleaning of metal cathodes using a hydrogen ion beam. *Phys. Rev. ST Accel. Beams*, 9, 063502.

Franklin, R. N. (2002). What significance does the Bohm criterion have in an active colisional plasma–sheath? *J. Phys. D: Appl. Phys.*, 35, 2270.

Franklin, R. N. (2002). You cannot patch active plasma and collisionless sheath. *IEEE Trans. Plasma Sci.* 30 (2002) 352.

Franklin, R. N. (2003). The plasma–sheath boundary region. *J. Phys. D: Appl. Phys.*, 36, R309.

Franklin, R. N. (2003). There is not such thing as a collisionally modified Bohm criterion. *J. Phys. D: Appl. Phys.*, 36, 2821.

Franklin, R. N. (2004). Where is the sheath edge? *J. Phys. D: Appl. Phys.*, 37, 1342.

Freton, P.; Gonzalez, J. J.; Camy Peyret, F. & Gleizes, A. (2003). Complementary experimental and theoretical approaches to the determination of the plasma characteristics in a cutting plasma torch. *J. Phys. D: Appl. Phys.*, 36, 1269.

Freton, P.;Gonzalez, J. J.; Gleizes, A.; Camy Peyret, F.; Caillibotte, G. & Delzenne, M. (2002). Numerical and experimental study of a plasma cutting torch. *J. Phys. D: Appl. Phys.*, 35, 115.

George, D. W. & Richards, P. H. (1968). Boundary conditions in wall-stabilized arc columns. *Brit. J. Appl. Phys. (J. Phys. D)*, 1, 1171.

Ghorui, S.; Heberlein, J. V. R. & Pfender, E. (2007). Non-equilibrium modelling of an oxygen–plasma cutting torch. *J. Phys. D: Appl. Phys.*, 40, 1966.

Girard, L.; Teulet, Ph.; Razafinimanana, M.; Gleizes, A.; Camy-Peyret, F.; Baillot, E. & Richard, F. (2006). Experimental study of an oxygen plasma cutting torch: I. Spectroscopic analysis of the plasma jet. *J. Phys. D: Appl. Phys.*, 39, 1543.

Goldston, R. J. & Rutherford, P. H. (1995). *Introduction to Plasma Physics*, Institute of Physics Publishing Bristol and Philadelphia IOP.

González-Aguilar, J.; Pardo, C.; Rodríguez-Yunta, A. & García Calderón, M. A. G. (1999). A theoretical study of a cutting air plasma torch. *IEEE Trans. Plasma Sci.*, 27, 264.

Guo, S.; Zhou, Q.; Guo, W. & Xu, P. (2010). Computational analysis of a double nozzle structure plasma cutting torch. *Plasma Chem. Plasma Process*, 30, 121.

Hackam, R. (1969). Total secondary ionization coefficients and breakdown potentials of hydrogen, methane, ethylene, carbon monoxide, nitrogen, oxygen and carbon dioxide between mild steel coaxial cylinders. J. Phys. B (Atom. Molec. Phys.), 2, 216.

Hill, R. J. & Jones, G. R. (1979). The influence of laminar and turbulent flows upon the electrical characteristics of wall-stabilised arcs. *J. Phys. D: Appl. Phys.*, 12, 1707.

Naghizadeh–Kashani, Y.; Cressault, Y. & Gleizes, A. (2002). Net emission coefficient of air thermal plasmas. *J. Phys. D: Appl. Phys.*, 35, 2925.

Nemchinsky, V. A. & Severance, W. S. (2006). What we know and what we do not know about plasma arc cutting. *J. Phys. D: Appl. Phys.*, 39, R423.

Nemchinsky, V. A. (1998). Plasma flow in a nozzle during plasma arc cutting. *J. Phys. D: Appl. Phys.*, 31, 3102.

Nemchinsky, V. A. (2009). A mechanism that triggers double arcing during plasma arc cutting. *J. Phys. D: Appl. Phys.*, 42, 205209.

Noble, B. (1964). *Numerical Methods: 2 Differences, Integration and Differential Equations*. Oliver and Boyd Ltd, Edinburgh.

Pardo, C.; González-Aguilar, J.; Rodríguez-Yunta, A. & Calderón, M. A. G. (1999). Spectroscopic analysis of an air plasma cutting torch. *J. Phys. D: Appl. Phys.*, 32, 2181.

Peters, J.; Heberlein, J. V. R. & Lindsay, J. (2007). Spectroscopic diagnostics in a highly constricted oxygen arc. *J. Phys. D: Appl. Phys.*, 40, 3960.

Prevosto, L.; Kelly, H. & Mancinelli, B. (2008). On the use of sweeping Langmuir probes in cutting arc plasmas–Part I: Experimental results. *IEEE Trans. Plasma Sci.*, 36, 263.

Prevosto, L.; Kelly, H. & Minotti, F. O. (2008). On the use of sweeping Langmuir probes in cutting arc plasmas–Part II: Interpretation of the results. *IEEE Trans. Plasma Sci.*, 36, 271.

Prevosto, L.; Kelly, H. & Minotti, F. O. (2009). An interpretation of Langmuir probe floating voltage signals in a cutting arc. *IEEE Trans. Plasma Sci.*, 37, 1092.

Prevosto, L.; Kelly, H. and Mancinelli, B. (2009). On the physical origin of the nozzle characteristic and its connection with the double-arcing phenomenon in a cutting torch. *J. Appl. Phys.*, 105, 013309.

Prevosto, L.; Kelly, H. and Mancinelli, B. (2009). On the space–charge boundary layer inside the nozzle of a cutting torch. *J. Appl. Phys.*, 105, 123303.

Raizer, Y. P. (1991). *Gas Discharge Physics*. Berlin, Germany: Springer.

Ramakrishnan, S.; Gershenzon, M.; Polivka, F.; Kearny, T. N. & Rogozinsky, M. W. (1997). Plasma generation for the plasma cutting process. *IEEE Trans. Plasma Sci.*, 25, 937.

Riemann, K–U. (1991). The Bohm criterion and sheath formation. *J. Phys. D: Appl. Phys.*, 24, 493.

Riemann, K–U. (2003). Kinetic analysis of the colisional plasma–sheath transition. *J. Phys. D: Appl. Phys.*, 36, 2811.

Shayler, P. J. & Fang, M. T. C. (1978). Radiation transport in wall-stabilized nitrogen arcs. *J. Phys. D: Appl. Phys.*, 11, 1743.

Sheridan, T. E. & Goeckner, M. J. (1995). Colisional sheath dynamics. *J. Appl. Phys.*, 77, 4967.

Sheridan, T. E. & Goree, J. (1991). Colisional plasma sheath model. *Phys. Fluids B*, 3, 2796.

Sternovsky, Z. & Robertson, S. (2006). Numerical solutions to the weakly colisional plasma and sheath in the fluid approach and the reduction of the ion current to the wall. *IEEE Trans. Plasma Sci.*, 34, 850.

van de Sanden, M. C. M., Schram, P. P. J. M.;.Peeters, A. G.; van der Mullen, J. A. M. & Kroesen, G. M. W. (1989). Thermodynamic generalization of the Saha equation for a two-temperature plasma. *Phys. Rev. A*, 40, 5273.

Zhou, Q.; Yin, H.; Li, H.; Xu, X.; Liu, F.; Guo, S.; Chang, X.; Guo, W. & Xu, P. (2009). The effect of plasma–gas swirl flow on a highly constricted plasma cutting arc. *J. Phys. D: Appl. Phys.*, 42, 095208.

Numerical Simulations of Physical and Engineering Processes

Edited by Prof. Jan Awrejcewicz

Numerical Simulations of Physical and Engineering Process is an edited book divided into two parts. Part I devoted to Physical Processes contains 14 chapters, whereas Part II titled Engineering Processes has 13 contributions. The book handles the recent research devoted to numerical simulations of physical and engineering systems. It can be treated as a bridge linking various numerical approaches of two closely inter-related branches of science, i.e. physics and engineering. Since the numerical simulations play a key role in both theoretical and application oriented research, professional reference books are highly needed by pure research scientists, applied mathematicians, engineers as well post-graduate students. In other words, it is expected that the book will serve as an effective tool in training the mentioned groups of researchers and beyond.

How to reference

In order to correctly reference this scholarly work, feel free to copy and paste the following:

Leandro Prevosto, Héctor Kelly and Beatriz Mancinelli (2011). On the Double-Arcing Phenomenon in a Cutting Arc Torch, Numerical Simulations of Physical and Engineering Processes, Prof. Jan Awrejcewicz (Ed.), ISBN: 978-953-307-620-1, InTech, Available from: http://www.intechopen.com/books/numerical-simulations-of-physical-and-engineering-processes/on-the-double-arcing-phenomenon-in-a-cutting-arc-torch

INTECH
open science | open minds